Quantum Josephson junction circuits and the dawn of artificial atoms

In 1985, experiments revealed the quantum behaviour of a macroscopic degree of freedom: the phase difference across a Josephson junction. The authors recount the history of this milestone for the development of superconducting quantum circuits.

John M. Martinis, Michel H. Devoret and John Clarke

Do macroscopic degrees of freedom obey quantum mechanics? During the first six decades of quantum mechanics the answer to this question was never addressed experimentally. Quantum mechanics was known to survive at the macroscopic level only through collective phenomena such as superfluidity, superconductivity, flux quantization and the Josephson effect. Although these phenomena are conventionally described as 'macroscopic', they are in fact classical manifestations on a macroscopic scale of the combination of large numbers of microscopic variables, each governed by quantum mechanics. The faceting of certain crystals, such as quartz, revealing the covalent bonds between constituent atoms, represents an elementary example of this class of quantum phenomena exhibited on a macroscopic scale.

In 1980, Anthony Leggett[1] emphasized the importance of distinguishing macroscopic quantum phenomena originating in the somewhat trivial large-scale accumulation of effects originating at the level of microscopic variables from those displayed, hypothetically, by a single macroscopic, collective degree of freedom. Although nothing in theory would seem to prevent such variables from fully obeying quantum mechanics, we felt challenged to see if it really was the case in practice.

In 1985, we answered the question with our experimental observation[2] of quantized energy levels of a current-biased Josephson junction[3,4]. Crucially, the measured values of the energy levels agreed quantitatively with quantum-mechanical predictions based on parameters of the junction that we had measured classically, in situ[5].

The Josephson tunnel junction consists of two superconductors separated by a thin insulating barrier through which Cooper pairs of electrons can tunnel coherently. For each superconductor, the density of Cooper pairs and their common phase describe its macroscopic quantum state. In the 1980s, Josephson junctions were used only in classical superconducting electronics devices, for example superconducting quantum interference devices (SQUIDs)[6] and the standard volt[7].

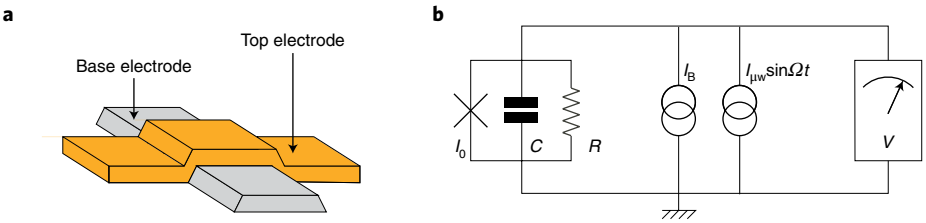

Fig. 1 | The Josephson junction and its measurement circuit. a, Schematic of a cross-strip Josephson superconducting tunnel junction. Our devices consist of a Nb base electrode and a top PbIn alloy electrode separated by a ~1-nm thick Nb-oxide layer formed by plasma-oxidation of the base electrode. **b**, Circuit schematic of a Josephson element (cross) shunted by a capacitance *C* and resistance *R*, and connected to both static bias (I_B) and microwave ($I_{\mu w}$) current sources. The voltage *V* across the junction is measured by a low-noise audio-frequency amplifier chain represented symbolically. Panel **b** adapted with permission from ref. [2], APS.

In our experiment, we investigated the behaviour of a single macroscopic variable — the phase difference δ between the two superconductors measured when there is zero static voltage across the barrier. Although the name phase difference might suggest a de facto quantum-mechanical variable, that is not the case. Crudely speaking, one can understand the phase difference as a sort of momentum of the centre of mass of Cooper pairs as they flow across a junction. It is a collective variable associated with all the electrons of the junction, like the charge on the electrodes of a capacitor.

For our experiments, we patterned Nb–NbO_x–PbIn tunnel junctions photolithograhically on oxidized Si chips in either a $10 \times 10\ \mu m^2$ or an $80 \times 10\ \mu m^2$ cross-strip geometry (Fig. 1a). To make measurements, as shown in Fig. 1b, we coupled each junction in turn to a static current source and a microwave source at frequency $\Omega/2\pi$ and used a low-noise amplifier to detect any voltage *V* developed. The junction is shunted by a capacitance *C*, which was dominated by the intrinsic junction capacitance, and a resistance *R*, which was dominated by contributions from the external circuitry.

The differential equation describing the dynamics of a Josephson junction with self-capacitance *C* can be shown to be equivalent to that for a particle of mass proportional to *C* moving in the one-dimensional tilted cosine potential[8,9], as shown in Fig. 2. The conductance R^{-1} determines the damping of the particle. For a junction with critical current (maximum supercurrent) I_0 biased with a current *I* just below I_0, the barrier height (Fig. 2) is $\Delta U = (4/3)\sqrt{2}U_0(1 - I/I_0)^{3/2}$ (ref. [10]), where $U_0 = I_0\Phi_0/2\pi$. The small oscillation frequency at the bottom of the well, also known as the plasma frequency $\omega_p/2\pi$ is given by $\omega_p = \omega_{p0}[1 - (I/I_0)^2]^{1/4}$. Here, $\omega_{p0} = (2\pi I_0/C\Phi_0)^{1/2}$ and $\Phi_0 = h/2e$ is the flux quantum, where *h* is the Planck constant and *e* the electronic charge. The plasma frequency quality factor is $Q = RC\omega_p \gg 1$.

Quantum mechanics predicts that the energy of the particle in the well is quantized, as indicated in Fig. 2. The 3/2 exponent in ΔU is associated with a cubic-shaped potential, which leads to a decrease in the spacing of the energy levels in the well

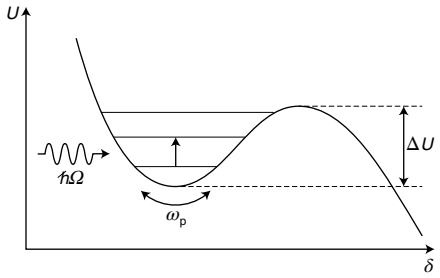

Fig. 2 | Cubic potential in which the macroscopic phase difference δ of the junction evolves quantum mechanically. Microwave irradiation at frequency $\Omega/2\pi$ induces transitions between the energy levels that quantum mechanics predicts to exist in the well. These transitions are detected by enhancement of the tunnelling rate, measured in the configuration of Fig. 1b. The transition frequencies are comparable with the plasma frequency $\omega_p/2\pi$. Figure adapted with permission from ref. [5], APS.

with increasing energy, as in the hydrogen atom. Increasing the bias current I also decreases the spacing of all the energy levels.

As we shall see, it is of central importance that the well be anharmonic. The quadratic potential of a simple harmonic oscillator leads to spacing between energy levels that is independent of level number for all quantum numbers. Conversely, transitions between levels of an anharmonic well with small quantum numbers can be straightforwardly resolved, unlike for large quantum numbers where Bohr's correspondence principle should always hold. As Leggett[1] has emphasized so eloquently, the use of an anharmonic oscillator enables one "to evade the correspondence limit".

The particle can escape from the well by two processes. In the classical limit $k_BT/\hbar\omega_p \gg 1/2\pi$ the particle escapes by thermal noise that activates it over the barrier; here k_B is the Boltzmann constant, T is temperature and $\hbar \equiv h/2\pi$. In this case, δ acts as a classical variable. In the quantum limit $k_BT/\hbar\omega_p \ll 1/2\pi$, on the other hand, the particle behaves as a wave packet, and the phase difference δ acts as a quantum operator rather than as a classical number. Since the tail of the wave packet extends under the barrier, the particle can escape by macroscopic quantum tunnelling through the barrier[11–14]. To verify the presence of quantized energy levels in the junction in the quantum regime, we aimed at measuring the enhancement of the tunnelling rate following transitions between the energy levels induced by microwave irradiation.

To compare our experimental results with theoretical predictions, we first used resonant activation[15] to measure the classical properties of each of our junctions in the same cool-down sequence. When a junction is current-biased below I_0 in its zero-voltage state with the particle localized in a potential well, thermal fluctuations modulate the angle of tilt of the washboard and cause the particle to be activated out of the well. For an underdamped junction, which has a hysteretic current–voltage characteristic, the particle runs down the washboard, creating a voltage across the junction. The fundamental idea of resonant activation is to apply microwaves with a power P at a frequency $\Omega/2\pi$ at or close to the plasma frequency, which is typically several GHz, to the junction in the classical (thermal) regime. This adds a small perturbation to the dynamics of the particle in the presence of thermal noise, increasing the activation rate of the particle out of the well and thereby reducing its lifetime τ. Within a few days of conceiving this idea, we verified the basic phenomenon with an analogue computer programmed to simulate a Josephson junction. Together with Daniel Esteve, we made computer simulations to show in more detail how one could extract parameters from this resonance.

We measured τ at 4.2 K as a function of I, P and Ω; Q and I_0 were inferred from different features of the thermal activation peak. To extract these parameters from the data accurately we first performed a numerical simulation of the junction in the presence of thermal noise. From the measurements and simulations of the junction in the presence of thermal noise we extracted ω_p and hence ω_{p0} and C; then $R = Q/\omega_pC$ — enabling us to make accurate measurements of all the relevant parameters in the classical regime. Further theoretical analyses[16,17] later confirmed our simulations.

Having obtained the values of the junction and circuit parameters, we were then in a position to measure quantized energy levels and compare their values with theoretical predictions with no fitted parameters. We made the measurements in the quantum limit at temperatures of a few tens of millikelvin.

The basis of the experiment was to measure the change in the escape rate $\Gamma(P) - \Gamma(0)$ of the junction from the zero-voltage regime as a function of the bias current I. We determined $\Gamma(0)$ and $\Gamma(P)$ separately by ramping the bias current repeatedly to obtain a histogram of the current at which the junction switched to the voltage state. We calculated the escape rates from the histograms, and then calculated $\Gamma(P) - \Gamma(0)$. Typically, we averaged over 10^5 switching events. We varied $\Gamma(0)$ from 10^2 to 10^5 s^{-1} and adjusted the microwave power P to produce $[\Gamma(P) - \Gamma(0)]/\Gamma(0) < 2$.

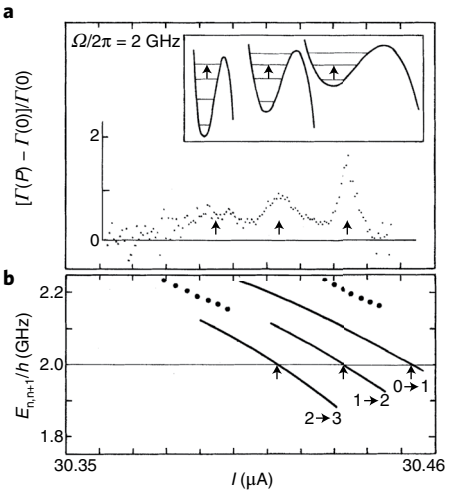

Fig. 3 | Resonances induced by microwaves at 2.0 GHz. a, $[\Gamma(P) - \Gamma(0)]/\Gamma(0)$ versus I for an 80×10 μm^2 junction at 28 mK ($k_BT/\hbar\Omega = 0.29$). Arrows indicate positions of resonances. Inset: corresponding transitions between energy levels. **b**, Calculated energy level spacings $E_{n,n+1}$ versus I for $I_0 = 30.572 \pm 0.017$ μA and $C = 47.0 \pm 3.0$ pF. Dotted lines indicate uncertainties in the 0→1 curve due to uncertainties in I_0 and C. Arrows indicate values of bias current at which resonances are predicted. Figure reproduced with permission from ref. [5], APS.

We expected the escape rate to be resonantly enhanced by microwaves, the frequency of which coincided with the spacing between two energy levels as compared with the rate in the absence of microwaves. Exciting the particle to the next higher energy level lowers the height and width of the effective barrier through which the particle must escape, increasing the escape rate. We searched for these resonances by varying the bias current to change the spacing while keeping the microwave frequency fixed. Figures 3 and 4 illustrate typical results.

In Fig. 3a we show the change in the escape rate induced by 2.0-GHz microwaves. The junction parameters were chosen so that the well contained several energy levels ($\Delta U/\hbar\omega_p \approx 6$), the lower excited states were significantly populated ($k_BT/\hbar\omega_p \approx 0.3$), and the damping was low enough ($Q \approx 80$) to produce narrow resonances. We directly observed these peaks in real time on the oscilloscope monitor, which displayed the current when the junction switched.

When one of us (J.M.M.) turned on the microwaves, three distinct values of

switching current became dominant, and he understood immediately that the computer plot would provide compelling evidence for quantized energy levels. The three peaks in $[\Gamma(P) - \Gamma(0)]/\Gamma(0)$ demonstrate that the escape rate is resonantly enhanced at specific values of the bias current. These discrete resonances are characteristic of transitions between quantized energy levels, as for example in the hydrogen atom, which set Niels Bohr on the path of quantum mechanics. The two peaks at the higher bias currents are approximately Lorentzian. No further peaks were observed at higher values of bias current.

To investigate the positions of these peaks we computed the energy levels by solving the Schrödinger equation numerically using the measured bias current and the values of I_0 and C obtained classically[13]. The solid lines in Fig. 3b indicate the calculated values of energy level spacings $E_{n,n+1}$ $(n = 0,1,2)$ versus I. The dotted lines indicate the uncertainty in the position of the $E_{0,1}$ curve arising from the estimated errors in I_0 and C. The uncertainties in the $E_{1,2}$ and $E_{2,3}$ curves are almost the same. The intersections of the curves with the horizontal 2.0-GHz line are the predictions of the bias currents at which the resonant peaks should occur. The absolute positions of the peaks agree with the predictions to within the experimental uncertainty. We note in particular that the separations of the peaks along the current axis are in excellent agreement with the quantum predictions.

In a second set of experiments we studied the dependence of $(E_1 - E_0)$ on the bias current for a junction with much lower values of I_0 and C that was more strongly in the quantum regime ($\Delta U/\hbar\omega_p \approx 2$, $k_B T/\hbar\omega_p \approx 0.1$). As before, we measured I_0 and C in the classical regime. Figure 4a shows resonances in $[\Gamma(P) - \Gamma(0)]/\Gamma(0)$ for four different microwave frequencies. In Fig. 4b we plot the predicted values of $(E_1 - E_0)$, along with the estimated uncertainty. The absolute measured positions of the peaks agree with the predictions to within the experimental uncertainties. The shift in the position of the resonance frequency as the microwave frequency is changed is in excellent agreement with predictions. Furthermore, the positions of the resonances are clearly very different from the classical prediction for the resonant activation of the particle oscillating at the plasma frequency $\omega_p/2\pi$ (dashed line), thus confirming the quantum character of the junction dynamics.

Following Leggett's pioneering theoretical lead, our experiment was the first to demonstrate convincingly the possibility of building artificial atoms that could be connected and controlled by electrical wires.

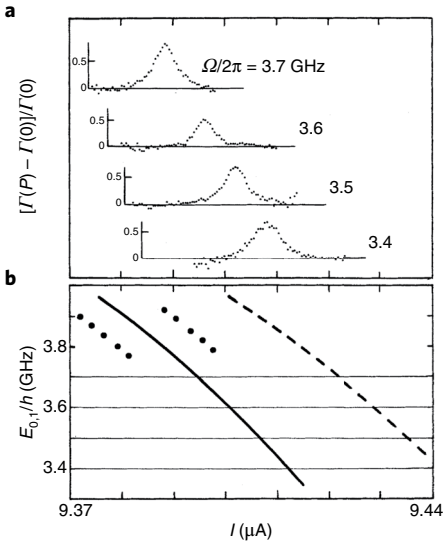

Fig. 4 | Resonances induced by microwaves at four different frequencies. a, $[\Gamma(P) - \Gamma(0)]/\Gamma(0)$ versus I for a 10 × 10 μm² junction at 18 mK. **b**, Calculated energy level spacing $E_{0,1}$ versus I for $I_0 = 9.489 \pm 0.007$ μA and $C = 6.35 \pm 0.4$ pF. Dotted lines indicate uncertainties in $E_{0,1}$ due to uncertainties in I_0 and C. Dashed line represents the plasma frequency. Figure reproduced with permission from ref. [5], APS.

Subsequently, an important step forward was the replacement of our niobium-based technology with Al–Al_2O_3–Al junctions. Although operating at a lower temperature, they are simpler to fabricate and have a much lower level of intrinsic dissipation than the Nb–NbO_x–PbIn junctions on which our experiment was based. It is now sometimes said that "aluminium is the silicon of superconductivity".

In due course, these artificial atoms enabled a wide variety of superconducting quantum bits (qubits), including circuits nicknamed 'Cooper pair box' (also known as a 'charge qubit')[18,19], 'flux qubit'[20,21], 'phase qubit'[22,23], 'quantronium'[24], 'transmon'[25,26] and 'fluxonium'[27]. In turn, qubits have enabled circuit quantum electrodynamics (QED) that addresses the quantum behaviour of the electromagnetic field, when microwave photons strongly interact with artificial atoms made from superconducting circuits.

One can also see circuit QED as an evolutionary step in the development of superconducting quantum circuits. It combines experiments on quantized energy levels of Josephson circuits coupled to those of a microwave cavity[28] with the microwave reflectometry approach of the radio-frequency single-electron transistor[29], in which one does not simply send a microwave signal to the circuit, but one also 'listens' to the signal coming back. Introductions to superconducting qubits and circuit QED can be found in various review articles, for example, refs. [30–33].

In contrast to cavity QED[34], in which photons interact with real atoms, the time scale for gates and readout is 1000 times faster in circuit QED. Currently, the state-of-the-art qubit decoherence rate is also 1,000 times faster, leading to comparable figures of merit, but circuit QED is able to acquire large amounts of data which is a particular advantage for correlation experiments. Consequently, tests of quantum principles can be performed that would not be feasible with real atoms, for example reversing a quantum jump[35]. With the advent of very fast electronics based on field-programmable gate arrays, combined with measurement-based feedback[36,37], circuit QED offers the unique opportunity of implementing full-fledged quantum-error correction[38], which will soon lengthen the coherence lifetime of a logical qubit way past the intrinsic coherence lifetime of its constituent parts. The 'break-even' point of quantum error correction — at which the lifetime of a qubit exceeds the lifetime of the constituents of the system — has been recently achieved for the first time in any platform[39].

Today, the successful interconnection of substantial numbers of superconducting qubits[40] heralds complex quantum circuits, which could in the future perform the full set of quantum tasks: sensing, communication, simulation, and computation. These quantum machines would likely complement, rather than replace, today's integrated circuits. For example, several teams have used superconducting quantum circuits to address the challenges associated with sensing spins[41,42], phonons[43] and exotic particles[44,45], quantum communication between different chips[46–48] or subsystems[49], transduction between microwave and optical photons[50], simulations of many-body systems[51] and computations of test algorithms (see the 'IBM experience' at https://go.nature.com/2HHNXDY). ❐

John M. Martinis[1,2,5], Michel H. Devoret[3,5] and John Clarke[4,5] ✉

[1]Department of Physics, University of California, Santa Barbara, CA, USA. [2]Google, Inc., Santa Barbara, CA, USA. [3]Department of Applied Physics, Yale University, New Haven, CT, USA. [4]Department of Physics, University of California, Berkeley, CA, USA. [5]These authors contributed equally: John M. Martinis, Michel H. Devoret, John Clarke.
✉*e-mail: jclarke@berkeley.edu*

Published online: 2 March 2020
https://doi.org/10.1038/s41567-020-0829-5

References

1. Leggett, A. J. *Prog. Theor. Phys. Suppl.* **69**, 80–100 (1980).
2. Martinis, J. M., Devoret, M. H. & Clarke, J. *Phys. Rev. Lett.* **55**, 1543–1546 (1985).
3. Josephson, B. D. *Phys. Lett.* **1**, 251–253 (1962).
4. Josephson, B. D. *Adv. Phys.* **14**, 419–451 (1965).
5. Martinis, J. M., Devoret, M. H. & Clarke, J. *Phys. Rev.* **35**, 4682–4698 (1987).
6. Clarke, J., Braginski, A. I. (eds) *The SQUID Handbook: Fundamentals and Technology of SQUIDs and SQUID Systems* (Wiley, 2004).
7. Rüfenacht, A., Flowers-Jacobs, N. E. & Benz, S. P. *Metrologia* **55**, S152–S173 (2018).
8. Stewart, W. C. *Appl. Phys. Lett.* **12**, 277–280 (1968).
9. McCumber, D. E. *J. Appl. Phys.* **39**, 3113–3118 (1968).
10. Fulton, T. A. & Dunkelberger, L. N. *Phys. Rev. B* **9**, 4760–4768 (1974).
11. Caldeira, A. O. & Leggett, A. J. *Ann. Phys.* **149**, 374–456 (1983).
12. Voss, R. F. & Webb, R. A. *Phys. Rev. Lett.* **47**, 265–268 (1981).
13. Jackel, L. D. et al. *Phys. Rev. Lett.* **47**, 697–700 (1981).
14. Devoret, M. H., Martinis, J. M. & Clarke, J. *Phys. Rev. Lett.* **55**, 1908–1911 (1985).
15. Devoret, M. H., Martinis, J. M., Esteve, D. & Clarke, J. *Phys. Rev. Lett.* **53**, 1260–1263 (1984).
16. Ivlev, B. I. & Mel'nikov, V. I. *Phys. Rev. Lett.* **55**, 1614–1617 (1985).
17. Larkin, A. I. & Ovchinnikov, Y. N. *J. Low. Temp. Phys.* **63**, 317–329 (1986).
18. Bouchiat, V., Vion, D., Joyez, P., Esteve, D. & Devoret, M. H. *Phys. Scr.* **T76**, 165–170 (1998).
19. Nakamura, Y., Pashkin, Y. A. & Tsai, J. S. *Nature* **398**, 786–788 (1999).
20. Mooij, J. E. et al. *Science* **285**, 1036–1039 (1999).
21. Chiorescu, I., Nakamura, Y., Harmans, C. J. & Mooij, J. E. *Science* **299**, 1869–1871 (2003).
22. Martinis, J. M., Nam, S., Aumentado, J. & Urbina, C. *Phys. Rev. Lett.* **89**, 117901 (2002).
23. Martinis, J. *Quant. Inf. Proc.* **8**, 81–103 (2009).
24. Vion, D. et al. *Science* **296**, 886–889 (2002).
25. Koch, J. et al. *Phys. Rev. A* **76**, 042319 (2007).
26. Houck, A. A. et al. *Phys. Rev. Lett.* **101**, 080502 (2008).
27. Manucharyan, V. E., Koch, J., Glazman, L. I. & Devoret, M. H. *Science* **326**, 113–116 (2009).
28. Devoret, M. H., Esteve, D., Martinis, J. M. & Urbina, C. *Phys. Scr.* **T25**, 118–121 (1989).
29. Schoelkopf, R. J., Wahlgren, P., Kozhevnikov, A. A., Delsing, P. & Prober, D. E. *Science* **280**, 1238–1242 (1998).
30. Clarke, J. & Wilhelm, F. K. *Nature* **453**, 1031–1042 (2008).
31. Girvin, S. M., Devoret, M. H. & Schoelkopf, R. J. *Phys. Scr.* **T137**, 014012 (2009).
32. Devoret, M. H. & Schoelkopf, R. J. *Science* **339**, 1169–1174 (2013).
33. Krantz, P., Kjaergaard, M., Yan, F., Orlando, T. P., Gustavsson, S. & Oliver, W. D. *Appl. Phys. Rev.* **6**, 021318 (2019).
34. Haroche, S. & Raimond, J.-M. *Exploring the Quantum: Atoms, Cavities and Photons* (Oxford Univ. Press, 2006).
35. Minev, Z. K. et al. *Nature* **570**, 200–204 (2019).
36. Sayrin, C. et al. *Nature* **477**, 73–77 (2011).
37. Vijay, R. et al. *Nature* **490**, 77–80 (2012).
38. Nielsen, M. A. & Chuang, I. L. *Quantum Computation and Quantum Information* Ch. 10 (Cambridge Univ. Press, 2000).
39. Ofek, N. et al. *Nature* **536**, 441–445 (2016).
40. Arute, F. et al. *Nature* **574**, 505–510 (2019).
41. Tabuchi, Y. et al. *Science* **349**, 405–408 (2015).
42. Ranjan, V. et al. *J. Mag. Res.* **310**, 106662 (2020).
43. Gustafsson, M. V., Santos, P. V., Johansson, G. & Delsing, P. *Nat. Phys.* **8**, 338–343 (2012).
44. Noguchi, A., Yamazaki, R., Tabuchi, Y. & Nakamura, Y. *Phys. Rev. Lett.* **119**, 180505 (2017).
45. Malnou, M. et al. *Phys. Rev. X* **9**, 021023 (2019).
46. Campagne-Ibarcq, P. et al. *Phys. Rev. Lett.* **120**, 200501 (2018).
47. Axline, C. et al. *Nat. Phys.* **14**, 705–710 (2018).
48. Kurpiers, P. et al. *Phys. Rev. Appl.* **12**, 044067 (2019).
49. Zhong, Y. P. et al. *Nat. Phys.* **15**, 741–744 (2019).
50. Higginbotham, A. P. et al. *Nat. Phys.* **14**, 1038–1042 (2018).
51. Ma, R. et al. *Nature* **566**, 51–57 (2019).

Acknowledgements

M.H.D. acknowledges support from the Army Research Office and Air Force Office of Scientific Research.